DETECTION OF CARBON MONOXIDE, CARBON DIOXIDE AND SULFUR DIOXIDE WITH PULSED TUNABLE $PbS_{1-x}Se_x$-DIODE LASERS

Bernd SUMPF, Dimitrii GÖRING, Rainer HASELOFF, Karin HERRMANN and Jens Wolfgang TOMM

Humboldt-Universität zu Berlin, Sektion Physik, Bereich Experimentelle Halbleiterphysik, Berlin 1 040, DDR

Received February 22, 1988
Accepted June 10, 1988

The purpose of this paper is to report our results on the detection and spectroscopic parameters of carbon monoxide, carbon dioxide and sulfur dioxide using high resolution linear diode laser spectroscopy with pulsed tunable $PbS_{1-x}Se_x$ homolasers. The parameters of pulsed diode lasers used in spectroscopy for various gases are discussed. The application of the diode laser spectrometer for CO gas detection at ppm level illustrates the sensitivity of the equipment.

The application of tunable lead salt diode lasers as radiation sources in the 300 to 3 000 cm^{-1} wavenumber region in high resolution spectroscopy of molecules and sensitive air pollution detection is known for years. The variety of experiments includes the Doppler-limited spectroscopy of molecules with the determination of line-positions, line-width, line-shape, line-strength and broadening coefficients as well as the detection of trace substances and gaseous pollutants in the atmosphere with ppb sensitivity[1-3].

This paper represents our results on some spectroscopic parameters of carbon monoxide, carbon dioxide and sulfur dioxide using diode laser spectroscopy with pulsed tunable $PbS_{1-x}Se_x$ homolasers. Generally the output wavenumber or wavelength of (Pb, Sn)(S, Se, Te) diode lasers with a given composition can be tuned quasicontinously by varying their operating temperature (coarse tuning) and/or the forward bias current (fine tuning). Both tuning mechanisms result from the strong temperature dependence of band-gap and refractive index in lead chalcogenide lasers. For a given operating temperature of the diode laser fine tuning is realized by constant (*cw*) or pulse bias current regime, which changes the amount of Joule heating and injected power in the active layer and finally the laser wavenumber $\tilde{\nu}_L$. For commercially available lead salt lasers *cw* operation is limited to temperatures less than 60 K, pulse operation is possible up to 120 K. These limits in operating temperature of laser diodes are a consequence of the lower level in the technology of lead salt lasers in comparison with III–V compound lasers.

The necessity of cryogenic cooling for lead salt lasers is a critical factor for technical applications and their temperature dependent operation regime (*cw* or pulse) determines the methods of signal detection. *Cw* operation at low temperatures enables selective and phase sensitive detection, allows to measure higher derivatives of the signal and to improve the signal-to-noise ratio efficiently. Alternatively, laser operation in periodic pulse regime[4,5] reduces the requirements for high quality laser parameters and makes possible maximum operating temperatures of about 120 K. For practical applications till now homodiode lasers are prefered with regard to their smaller degradation during cooling cycles.

RESULTS AND DISCUSSION

Laser Properties and Tuning Mechanism

$PbS_{1-x}Se_x$ homojunction material is produced according to a method described elsewhere[6]. An ohmic contact layer system containing palladium, gold and indium is obtained by means of an reductive and autocatalytic method[7]. Fabry–Perot single diode lasers are formed by cleaving along the (100)-crystal surfaces. Typical dimensions of a laser are $(200 \times 400 \times 300)\ \mu m^3$. The mounting of laser diodes in a special package was accomplished by indium soldering. Maximum operating temperatures of 120 K are obtained for pulsed diode lasers with medium carrier concentrations (about $10^{18}\ cm^{-3}$) and high mobilities ($10^4\ cm^2/Vs$) in the *n*-type bulk material, into which the *p*–*n*-junction is formed by isothermal selenium diffusion[6]. For spectroscopic investigations of CO_2, SO_2, and CO in the wavenumber region from 2 080 cm^{-1} to 2 380 cm^{-1} $PbS_{1-x}Se_x$ lasers were applied with the following x compositions: $x = 0$, $x = 0{\cdot}2$, $x = 0{\cdot}32$.

Figure 1 shows the temperature dependence of the threshold current density for such a group of diode lasers. Since single mode emission of a diode laser is often obtained near by the threshold current i_s, from Fig. 1 follow the spectroscopic operating parameters of our diode lasers (Table I). High resolution spectroscopy using pulsed diode lasers (with the characteristic parameters diode current i, pulse duration τ and pulse repetition rate f) is based on the fine tuning of laser wavenumber within one pulse. Figure 2 shows this principally. During one pulse with a current i just above the threshold current (Fig. 2*a*) the laser temperature T_0, which usually slightly differs from the cooling temperature T_{cryost}, increases slowly to $T_0 + \Delta T(\tau)$ as a consequence of Joule heating of the diode (Fig. 2*b*). Between two neighbouring pulses the original temperature T_0 is returned. This fine tuning of laser temperature causes the fine tuning of laser wavenumber $d\tilde{\nu}/dt$ for one mode or the hopping from one mode to another (Fig. 2*c*), because wavenumber or band-gap energy is in lead salts strongly temperature dependent[1]. Even weak absorption lines of different molecules are detectable within one pulse (Fig. 2*d* with strong absorption line). Usually the

TABLE I

Parameters of $PbS_{1-x}Se_x$ lasers for spectroscopic investigations

Type	x	T K	$\tilde{\nu}$ cm^{-1}	i A	τ μs	f Hz	D $cm^{-1}\,\mu s^{-1}$
I	0	10	2 300	2·1	20	100	0·05 ± 0·01
II	0·2	80	2 290	3·2	6	100	0·26 ± 0·05
III	0·32	80	2 140	3·0	10	100	0·002 ± 0·005

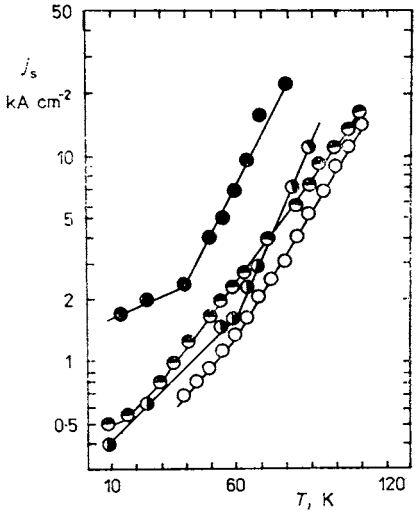

FIG. 1

Dependence of the threshold current density on temperature for lasers applied in spectroscopic experiments. ◑ $PbS_{0.8}Se_{0.2}$; ● PbS; ◓, ○ $PbS_{0.68}Se_{0.32}$

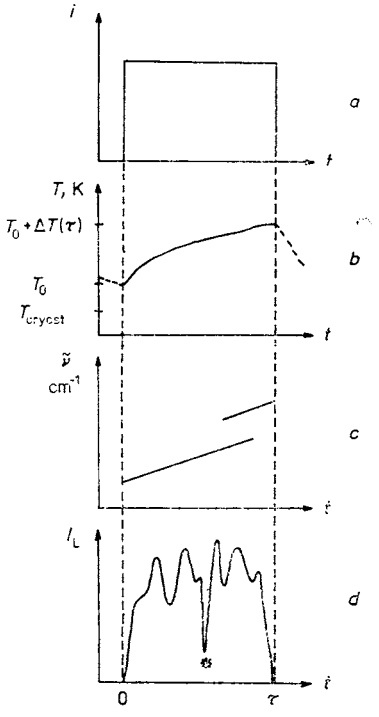

FIG. 2

Mechanism of single mode tuning of a pulsed diode laser by thermal heating at a fixed temperature of the cryostat: *a* current pulse, *b* change in temperature during the pulse, *c* tuning of wavenumber within one mode and mode hopping caused by the change in temperature, *d* laser intensity measured (with a strong absorption line (*) and etalon marks)

periodic interference picture of a germanium etalon as relative wavenumber calibration superposes the pure absorption picture (Fig. 2*d*), which enables to determine the line spacing. For our conditions the fine tuning was determined using various germanium-Fabry–Perot etalons with 4, 6, and 20 mm thickness, respectively. The distance between the extrema of interference is 0·31, 0·21, and 0·006 cm^{-1}, respectively. In this way the fine tuning rate may be obtained easily by measuring the distance between the extrema of interference using an oscilloscope. The laser parameters of $PbS_{1-x}Se_x$ diodes applied in spectroscopy are given in Table I.

The theoretical description of the three-dimensional heat transfer in pulsed diode lasers demands numerical methods. For the simple one-dimensional case, Zasavitzky[8] determined the temperature increase ΔT in a diode during one pulse. After starting the pulse the active layer with thickness d_{act} is heated adiabatically and the temperature increase ΔT varies with time t as:

$$\Delta T(t) = a_1 t \quad \text{for} \quad 0 < t < d_{act}^2/16D_T \,. \tag{1}$$

If heat transfer becomes efficient ΔT changes not linearly with t but with a square-root law

$$\Delta T(t) = a_2\sqrt{t} - b \quad \text{for} \quad t > d_{act}^2/16D_T \,. \tag{2}$$

In both equations D_T is the thermal diffusion coefficient, a_1 and a_2 are parameters which depend on the diode current I, the voltage U at the junction, the heat conductivity $\varkappa$, the heat capacity c_p, the laser cross section A, the external quantum efficiency η_{ext} and other parameters mentioned above:

$$a_1 = \frac{IU(1 - \eta_{ext})}{c_p d_{act} A} \tag{3}$$

$$a_2 = \frac{IU(1 - \eta_{ext})}{\varkappa A} \sqrt{\frac{D_T}{\pi}} \,. \tag{4}$$

The constant b in Eq. (2) represents the time independent contribution to the temperature change ΔT, which is determined from the equilibrium between heat production within the pulses and the constant heat drain through the contacts. The validity of Eq. (1) or Eq. (2) was proved by measuring the tuning rate $D = d\tilde{\nu}/dt$ for the single modes of a laser according to Fig. 2*c*. For a diode laser with Fabry–Perot cavity (refractive index $\bar{n}$, operating temperature $T = T_0 + \Delta T$, where $T_0 \geqq T_{cryost}$) the tuning rate D of a single laser mode is for $t > d_{act}^2/16D_T$ given by

$$D(\tilde{\nu}, t) = \left.\frac{d\tilde{\nu}}{dt}\right|_T = \tilde{\nu} \frac{1}{\bar{n}(\tilde{\nu}, T)} \frac{d\bar{n}(\tilde{\nu}, T)}{dt} \frac{a_2}{2\sqrt{t}} \,. \tag{5}$$

Measuring the time evaluation of the tuning rate D within one pulse at a fixed temperature T we found for $PbS_{1-x}Se_x$ homolasers and $Pb_{1-x}Sn_xTe$ heterolasers a good agreement with the square-root similar law according to Eq. (2) or (5). The experimental values for a_2 and b from tuning rate at 80 K and the calculated values for a_2 are represented in Table II. Figure 3 shows a typical temporal evolution of the laser power within a pulse. The influence of the etalon is obvious and a tuning rate $D = 0{\cdot}06\ \mathrm{cm^{-1}\ \mu s^{-1}}$ was determined. D is a function of the current I and the temperature T, too. We found for a resistance–area-product RA larger than $6 \cdot 10^{-4}\ \Omega\ \mathrm{cm^2}$ a quadratic law $D \sim I^2$ and for RA smaller than $6 \cdot 10^{-4}\ \Omega\ \mathrm{cm^2}$ a linear dependence $D \sim I$. Here R is the diode resistance at the current I. This rule is valid for temperatures below 40 K, where the tuning rate only weakly depends on the temperature.

Description of the Laser Spectrometer

The basic idea of the spectrometer is that by varying the optical arrangement, simple laser tests and spectroscopic measurements may be carried out. This variation includes the investigation of high resolution spectra in the laboratory and over long pathes in free atmosphere. Figure 4 shows the arrangement of the spectrometer.

The tunable diode laser is situated in a highly temperature stable helium cryostate (stability about 10^{-3} K) which may be replaced by a simple N_2 cryostat in the case of technical application. Additional temperature stabilization as described in ref.[4] is not used. The tunable diode laser is operating with current pulses up to 5 A for spectroscopic measurements and up to 20 A for laser tests. Typical pulse durations τ are 3–30 μs and typical frequencies f are 100–200 Hz. Pulse magnitude, duration and frequency may be varied within 256 steps by a microcomputer or continuously by a commercial pulse generator (duration 0·4–100 μs, frequency 10–2 500 Hz).

The optical imaging system (see Fig. 4*a*) consists of BaF_2 and CaF_2 lenses with focal lengths of 10–15 cm. The gas-cells used have a diameter of 35 mm and a length

TABLE II

Change in laser temperature $T = T_0 + \Delta T$ ($T_0 \geqq T_{cryost}$) during the excitation pulse for a $PbS_{0.8}Se_{0.2}$ diode laser at $T_{cryost} = 80$ K

i A	T_0(exp.) K	a_2(exp.) $\mathrm{K\ \mu s^{-1/2}}$	a_2(Eq. (4)) $\mathrm{K\ \mu s^{-1/2}}$
3	83·2	2·4	2·34
3·5	85·0	2·3	2·73
4	85·3	2·8	3·12
4·5	85·0	3·0	3·51
5	85·0	4·0	3·90

TABLE III

Necessary tuning rates for the detection of absorption lines

Measurement	$\Delta\tilde{\nu}_H$, cm^{-1}	D, $cm^{-1}\ \mu s^{-1}$	
		to detect a line	to analyse a line
Doppler broadened			
CO line at 2 145 cm^{-1}	0·005	0·05	0·01
CO_2 line at 2 349 cm^{-1}	0·0043	0·043	0·009
SO_2 line at 2 499 cm^{-1}	0·0039	0·039	0·008
SO_2 line at 1 360 cm^{-1}	0·0021	0·021	0·004
pressure broadened (p = 100 kPa)			
CO line at 2 145 cm^{-1}	0·13	1·3	0·26
CO_2 line at 2 349 cm^{-1}	0·12	1·2	0·24

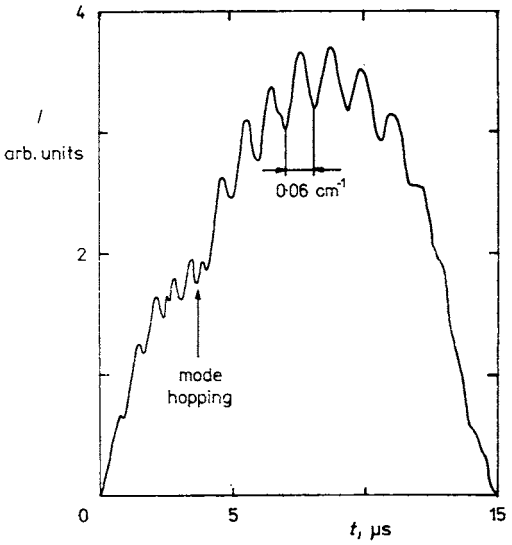

FIG. 3

Temporal evolution of the laser power within one pulse superposed by germanium etalon marks, multimode regime of a PbS homolaser

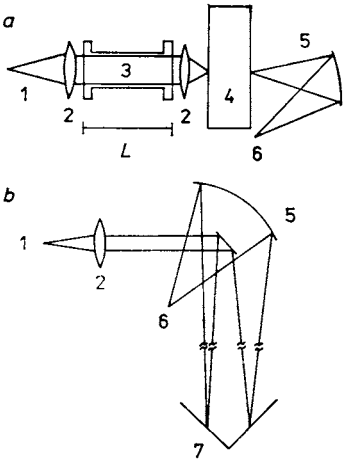

FIG. 4

Optical imaging system: *a* for measurements in laboratory, *b* for measurements over long pathes in free atmosphere. 1 laser, 2 lense, 3 gas cell, 4 monochromator, 5 mirror, 6 photodiode, 7 retroreflector

of 515 mm, 1 500 mm, and 2 015 mm. Thus weaker absorption lines may be detected under laboratory conditions, too. For mode selection an SPM 2 grating monochromator was used (see Fig. 4*a*). The signal from the monochromator was focussed on the detector using a spherical mirror. The optical imaging system for measurements in free atmosphere is also based on BaF_2 and CaF_2 lenses. After forming a parallel beam the signal passes the long path. The retroreflector is a triple mirror. After passing the long path the signal is focussed on the detector by a spherical mirror. All optical elements except the retroreflector are mounted on one common slab. Using this construction we detected gases over path lengths up to 300 m.

For signal detection PbTe, $Pb_{1-x}Sn_xTe$ and $Hg_{1-x}Cd_xTe$ photodiodes cooled at 80 K were used. The time constant of the detector–amplifier-system was 100 ns. Taking into account the well-known widths of the absorption lines of the gases one can calculate the demands to the tuning rates to ensure the detection of single lines (Table III). Further processing of the signal is made using a boxcar integrator and a microcomputer. The digitalization of the signal and the temperature (voltage from a thermocouple) is implemented with a 10 bit analog-digital-converter. By choice the absolute temperature or the difference from a selected temperature may be measured.

Spectroscopic Investigations and Gas Detection in Atmosphere

The intensity of a given laser beam I_L at a certain wavenumber $\tilde{\nu}$ after passing an absorbing medium is given by Lambert–Beer law. Assuming that the absorption coefficient could be separated into two parts, we distinguish one part which depends on the wavenumber and causes the line structure within the spectrum $\alpha(\tilde{\nu})$ and a second one α_0, which is constant within the wavenumber interval of laser emission. For the intensity $I_L(\tilde{\nu})$ we can write:

$$I_L(\tilde{\nu}) = I_0(\tilde{\nu}) \exp(-\alpha_0 CL) \exp\langle -\alpha(\tilde{\nu})\, CL\rangle \qquad (6)$$

$I_0(\tilde{\nu})$ is the intensity of the laser beam without absorption, α the absorption coefficient, measured in m^{-1}/ppb, C is the concentration, measured in ppb, and L is the pathlength. To determine the concentration of a known substance we measure the laser intensity at the maximum of an absorption line $I_L(\tilde{\nu}_0)$ (time point A0 in Fig. 8) and the laser intensity I_L at the time points A1 and A2, i.e. $I_L(\tilde{\nu}_0 - \delta\tilde{\nu})$ and $I_L(\tilde{\nu}_0 + \delta\tilde{\nu})$. The latter we use to fix the intensity $I_0(\tilde{\nu}_0)\exp(-\alpha_0 CL)$ caused by the background absorption at $\tilde{\nu}_0$ which is assumed to be the mean value of $I_L(\tilde{\nu}_0 + \delta\tilde{\nu})$ and $I_L(\tilde{\nu}_0 - \delta\tilde{\nu})$. Knowing the absorption coefficient $\alpha(\tilde{\nu}_0)$ and the pathlength L we obtain the concentration using:

$$C = \frac{1}{\alpha(\tilde{\nu}_0)\, L} \ln \frac{2I_L(\tilde{\nu}_0)}{I_L(\tilde{\nu}_0 + \delta\tilde{\nu}) + I_L(\tilde{\nu}_0 - \delta\tilde{\nu})}. \qquad (7)$$

Applying this method turbulences in atmosphere are excluded, because their time constant is greater than the time difference between the three points, necessary for measuring.

Equation (7) demands lasers working in a single mode regime. In a multimode regime, the intensities of the other modes I_M have to be considered and

$$C = \frac{1}{\alpha(\tilde{\nu}_0)\, L} \ln \frac{2\langle I_L(\tilde{\nu}_0) - I_M \rangle}{I_L(\tilde{\nu}_0 + \delta\tilde{\nu}) + I_L(\tilde{\nu}_0 - \delta\tilde{\nu}) - 2I_M} \tag{8}$$

provides the correct value.

The absorption coefficient of one absorption line could be described by

$$\alpha(\tilde{\nu}) = S\Phi(\tilde{\nu} - \tilde{\nu}_0)\,, \tag{9}$$

where S is the integrated line-strength (cm^{-2}/ppm) and $\Phi(\tilde{\nu} - \tilde{\nu}_0)$ is the line profile (for a further detailed discussion see refs[9,10]). Usually the line profile is given as a Voigt profile

$$\Phi(\tilde{\nu} - \tilde{\nu}_0) = \frac{2}{\Delta\tilde{\nu}_D} \sqrt{\left(\frac{\ln 2}{\pi}\right)} \frac{a}{\pi} \int_{-\infty}^{+\infty} \frac{\exp(-y^2)}{a^2 + (x - y)^2}\, dy\,, \tag{10}$$

where y is an integration parameter and a is the Voigt parameter

$$a = \sqrt{\ln 2}\, \frac{\Delta\tilde{\nu}_C}{\Delta\tilde{\nu}_D}\,, \tag{11}$$

x is the distance from the line centre

$$x = 2\, \frac{\sqrt{\ln 2}}{\Delta\tilde{\nu}_D} (\tilde{\nu} - \tilde{\nu}_0)\,, \tag{12}$$

$\Delta\tilde{\nu}_D$ is the Doppler-width ($FWHM$)

$$\Delta\tilde{\nu}_D = 7{\cdot}162 \,.\, 10^{-7} \tilde{\nu}_0 \sqrt{(T/M)} \tag{13}$$

$\Delta\tilde{\nu}_D$, $\tilde{\nu}_0$ in cm^{-1}; T in K; M in g mol^{-1}.

The collision broadening ($FWHM$) can be described as

$$\Delta\tilde{\nu}_C = 2\gamma_{g-h} p\,, \tag{14}$$

where $2\gamma_{g-h}$ is the broadening coefficient for collisions between the gas g, which causes the absorption line and the other gas h, whose molecules collide with the

molecules of the gas g. Under the condition $\Delta\tilde{\nu}_C \gg \Delta\tilde{\nu}_D$ the Voigt profile provides the Lorentz profile, in the case $\Delta\tilde{\nu}_C \ll \Delta\tilde{\nu}_D$ it becomes Gaussian.

For linewidths $\Delta\tilde{\nu}_H$ measured at pressures where collision and Doppler broadening have to be taken into account the following approximation could be used[11]:

$$\frac{\Delta\tilde{\nu}_H^2 - \Delta\tilde{\nu}_D^2}{\Delta\tilde{\nu}_H} = 2\gamma_{g-h}p \,. \qquad (15)$$

At high pressure $\Delta\tilde{\nu}_H$ is equal to $\Delta\tilde{\nu}_C$.

Line Broadening, Line Shape Measurements and Gas Detection

Fundamental band of carbon monoxide gas detection at ppm *level.* For these investigations we used lasers of type *II* (at 40 K) and type *III* (at 80 K) (see Table I). Type II is only used to calibrate the monochromator with the help of known CO absorption lines. By changing temperature and excitation we could detect 25 lines from 2 180 cm^{-1} ($R(9)$) to 2 080 cm^{-1} ($P(17)$) with only one laser. All other measurements were carried out with diode lasers of type *III*.

Figure 5 shows the $R(6)$ CO absorption line at a total pressure of 0·7 kPa. The line profile is determined by Doppler broadening and is in good agreement with the theoretical values (Eq. (*10*)).

Figure 6 illustrates the pressure dependence of the line width for the $R(6)$ line. Analogous experiments were carried out for the $R(7)$ and $R(9)$ lines. By measuring the halfwidth and using Eq. (*15*) we obtained the broadening coefficient $2\gamma_{CO-air}$ for these lines. The results are summarized in Table IV.

Lasers of type *III* were also used to measure CO-concentrations in atmosphere, applying a modified electronic equipment[13]. The concentration was calculated according to Eq. (*7*).

Figure 7 shows the obtained time dependence of CO-concentration in free atmosphere for a pathlength of 100 m. It was possible to detect CO gas at a concentration as low as 0·1 ppm (background level) with a certainty of 0·01 ppm. The longest pathlength we obtained was achieved during an experiment made with IOFAN/ /Moscow and FIAN/Moscow in the G.D.R.. It was possible to detect CO over a path of 1 200 m at background level.

Carbon dioxide ν_3*-band, gas detection in respiratory gases.* Only a short pathlength is needed to detect carbon dioxide because of the large value of the absorption coefficient of 0·001 cm^{-1}/ppm at 2 450 cm^{-1} for the strongest lines[14] and the high natural concentration of 300 ppm (ref.[15]). For the measurement of CO_2 concentration in respiratory gases only a pathlength of 10 cm was needed. Figure 8 shows such a measurement with a type *II* diode laser at 80 K. In point A0 the absorption line $P(50)$ at 2 302 cm^{-1} is situated within one laser mode. Point B shows the super-

position of mode hopping and the (assumed) absorption line $P(58)$ at 2 295 cm^{-1}. Only in the first case exact concentration measurements are possible.

If the natural CO_2 concentration in the atmosphere outside the gas cell and the absorption coefficient for the weak line $P(50)$ are known or measured it is possible to determine the respiratory concentration of CO_2 in the gas cell. For curve *II* 6 000 ppm and for curve *III* 12 000 ppm were determined, using Eq. (*7*) and $\alpha(\tilde{\nu}_0) =$

TABLE IV
Broadening coefficients in the CO fundamental band

Line	$2\gamma_{CO-air}$(300 K), 10^{-5} cm^{-1} Pa^{-1}		
	ref.[10]	ref.[12]	our results
$R(6)$	0·124	0·119 ± 0·008	0·120 ± 0·002
$R(7)$	0·128	0·118 ± 0·002	0·125 ± 0·005
$R(8)$	0·123	0·122 ± 0·008	
$R(9)$	0·119	0·116 ± 0·010	0·112 ± 0·013

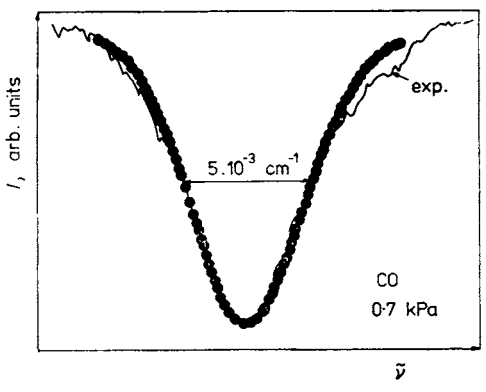

FIG. 5
Doppler broadened CO absorption line $R(6)$ at 2 165·6 cm^{-1}, ● theoretical values

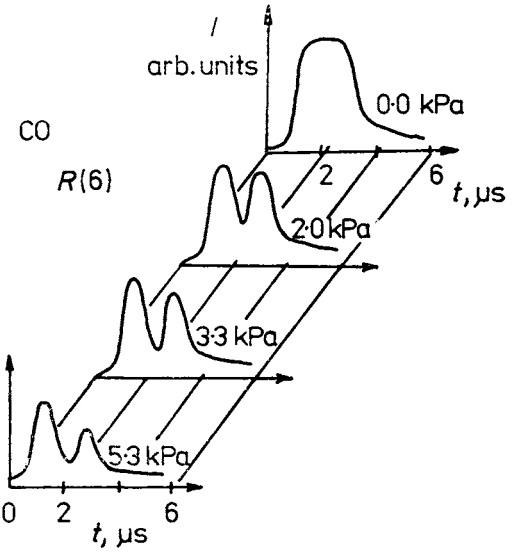

FIG. 6
Dependence of linewidth on total pressure for the carbon monoxide line $R(6)$

$= 1 \cdot 10^{-5}$ cm^{-1}/ppm. The measurements provide also values for the line broadening at the atmospheric pressure. With a tuning rate of 0·26 cm^{-1} μs^{-1} the line width is equal to 0·11 cm^{-1} in good agreement with other authors[16,17].

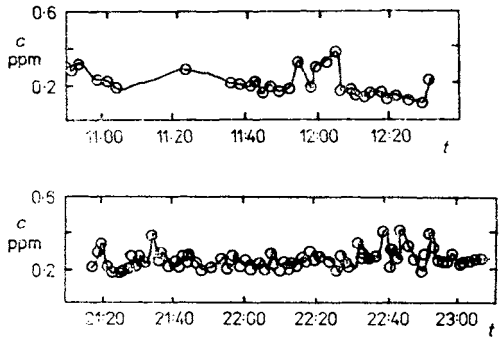

FIG. 7

Changes in CO concentration in free atmosphere measured with diode laser spectrometer

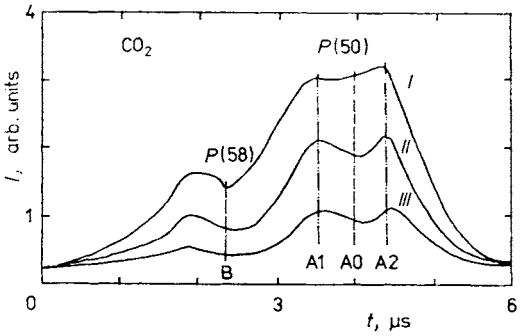

FIG. 8

Carbon dioxide gas detection in respiratory gases near 2 302 cm^{-1} ($P(50)$): *I* measured intensity without gas in the gas cell, *II* with air containing 6 000 ppm CO_2 (exp. determined value), *III* with air containing 12 000 ppm CO_2 (exp. determined value)

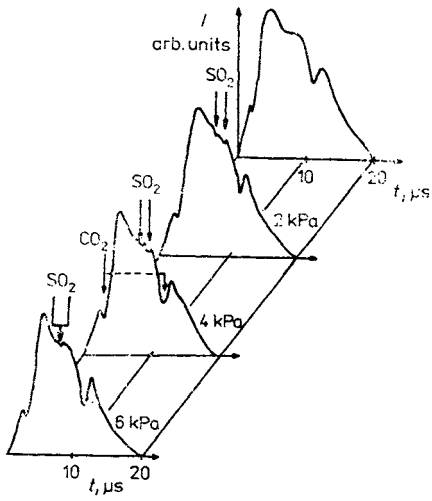

FIG. 9

Dependence of linewidth on total pressure for carbon dioxide and sulfur dioxide at 2 290 cm^{-1}

A further investigation of CO_2 at 2 290 cm^{-1} with diode *I* at 10 K shows Fig. 9. The dependence of the linewidth on pressure provides a pressure broadening coefficient of $2\gamma_{CO_2-air} = (0{\cdot}109 \pm 0{\cdot}005)\ 10^{-5}\ cm^{-1}\ Pa^{-1}$.

Sulfur dioxide $2\nu_1$ *band.* Figure 9 shows not only two strong CO_2 lines, but also two weak lines of the $2\nu_1$ band of sulfur dioxide. These lines have absorption coefficients of $7 . 10^{-9}\ cm^{-1}$/ppm, which are 700 times smaller than the absorption coefficients of the strongest line in the ν_3 band of SO_2 at 1 360 cm^{-1} with $3{\cdot}5 . . 10^{-6}\ cm^{-1}$/ppm (ref.[18]). Nevertheless a pathlength of 2 m was sufficient to detect these lines.

Trying to determine the pressure broadening coefficient we obtained $2\gamma_{SO_2-air} = (0{\cdot}30 + 0{\cdot}03)\ 10^{-5}\ cm^{-1}\ Pa^{-1}$. For pressures above 20 kPa single lines could not be detected because of line superposition. Since values for $2\gamma_{SO_2-air}$ in the $2\nu_1$ band from other authors were not available, we can only compare our results with those of Hinkley for the ν_1 band[19] or of Osumi for the ν_1 band and the ν_3 band (ref.[18]). The first value is $2\gamma = 0{\cdot}3 . 10^{-5}\ cm^{-1}\ Pa^{-1}$ and the latter $0{\cdot}207 . 10^{-5}\ cm^{-1} . . Pa^{-1}$. Own results in the ν_3 band provide the value of $(0{\cdot}23 \pm 0{\cdot}03) . 10^{-5}\ cm^{-1} . . Pa^{-1}$.

CONCLUSION

Our results show the capability of a simple experimental arrangement with pulsed diode lasers to study molecular parameters of gases and to detect molecular gases at the ppm level.

The diffused homolasers meet all necessary demands for the application in high sensitive gas detection. Working temperatures of 80 K are possible. Beside the results described here we examined methan, sulfur dioxide and water vapour near 1 370 cm^{-1}. These results will be discussed later on[20].

The authors wish to thank Mr. Götz Lindenberg for providing the laser crystals and Dr A. Szczerbakow (Instytut Fizyki, PAN, Warszawa. Poland) for the helpfull discussion to improve the laser parameters.

REFERENCES

1. Eng R. S., Butler J. F., Linden K. J.: Opt. Engn. *19*, 945 (1980).
2. Hinkley E. D., Nill K. W., Blum F. A. in: *Topics in Applied Physics, Laserspectroscopy of Atoms and Molecules* (H. Walther, Ed.), p. 155. Springer, Berlin 1976.
3. *Proceedings of the IXth International Conference on High Resolution Infrared Spectroscopy, Liblice, September 8—12, 1986*; abstract No. LM 10, LT 6, LT 8 and others.
4. Zasavitzky I. I., Kusnezov A. I., Kosichkin Yu. V., Kryukov P. V., Nadeshdinskii A. I., Perov A. H., Stepanov E. V., Shotov A. P.: Pisma Zh. Eksp. Teor. Fiz. *8*, 1168 (1982).
5. Zasavitzky I. I., Kosichkin Yu. V., Nachutin A. I., Okunzev N. Yu., Perov A. N., Shotov A. P.: *IOFAN Preprint* Nr. 14, Moscow 1985.

6. Tomm J. W., Sumpf B., Herrmann K., Szczerbakow A.: Cryst. Res. Technol. *22*, 981 (1987).
7. Herrmann K., Sumpf B., Böhme D., Hannemann M.: Cryst. Res. Technol. *18*, 1083 (1983).
8. Zasavitzky I. I., Kosichkin Yu. V., Perov A. N., Polyakov Yu. A., Shirokov A. M., Shotov A. P.: *FIAN Preprint* Nr. 150, Moscow 1981.
9. Penner S. S.: *Quantitative Molecular Spectroscopy and Gas Emissivities.* Pergamon Press, London 1959.
10. Varghese P. L., Hanson R. K.: J. Quant. Spectrosc. Radiat. Transfer *26*, 339 (1981).
11. Sun J. N. P., Griffiths P. R.: Appl. Opt. *20*, 1691 (1981).
12. Varanasi P.: J. Quant. Spectrosc. Radiat. Transfer *15*, 191 (1975).
13. Bobey C., Dudeck I.: Radio Fernsehen Elektronik *36*, 520 (1987).
14. Reid J., Garside B. K., Shewchun J.: Opt. Quant. Electron. *11*, 385 (1979).
15. *ABC Umweltschutz*, 3. Auflage. VEB Deutscher Verlag für Grundstoffindustrie, Leipzig 1984.
16. Arie E., Lacome N., Arcas P., Levy A.: Appl. Opt. *25*, 2584 (1986).
17. Devi V. M., Fridovich B., Jones G. D., Snyder D. G. S.: J. Mol. Spectrosc. *105*, 61 (1985).
18. Osumi M., Kunitomo T.: J. Quant. Spectrosc. Radiat. Transfer *21*, 343 (1979).
19. Hinkley E. D., Calawa A. R., Kelley P. L., Clough S. A.: J. Appl. Phys. *43*, 3222 (1972).
20. Sumpf B., Herrmann K., Kühnemann F.: Unpublished results.